Environ Earth Sci (2015) 74:5971–5988
DOI 10.1007/s12665-015-4622-1

ORIGINAL ARTICLE

Quantitative interpretation of magnetic anomalies from bodies approximated by thick bed models in complex environments

Lev V. Eppelbaum[1]

Received: 18 November 2014 / Accepted: 7 June 2015 / Published online: 23 June 2015

Abstract Magnetic prospecting is a rapid and inexpensive geophysical tool and one of the most widely used methods for geophysical prospection throughout the world. However, the noise factors—such as inclined magnetization, complex geological structure of investigated areas, and uneven terrain relief—strongly obscure the interpretation of observed magnetic anomalies. The developed methodology of magnetic anomalies' interpretation from models of thin beds and horizontal circular cylinders (spheres) in complex environments (oblique magnetization, rugged relief and unknown levels of the normal magnetic field) using improved versions of characteristic points and tangents was presented in detail in the author's previous publications. However, many geological targets have a geometrical form of thick beds and thin horizontal plates and intermediate forms that crop up between these two models. In this paper, a methodology for interpreting magnetic anomalies produced by thick bed models in complex environments is explicitly described. It shows that quantitative analysis of magnetic anomalies due to intermediate targets could be successfully carried out using the methodology developed for the thick bed model. In the case of a thin horizontal plate with a large horizontal size, two distinct anomalies (from the left and right ends) may be interpreted as anomalies from thin beds. The interpretation methodology was successfully tested, both on typical models and on real geological targets. It was concluded that these methods could be effectively applied for quantitative analysis of magnetic surveys for geological–geophysical mapping, archeological target delineation, ore body searching, revealing oil and gas traps, and solving other geological and environmental problems.

✉ Lev V. Eppelbaum
levap@post.tau.ac.il

[1] Department of Geosciences, Tel Aviv University, Ramat Aviv, 69978 Tel Aviv, Israel

Keywords Magnetic anomalies · Oblique magnetization · Rugged relief · Quantitative analysis · Thick bed · Intermediate model · Horizontal plate

Introduction

Magnetic prospecting has been successfully applied to geological–geophysical mapping, searching for useful minerals, and solving various environmental problems, as it is a rapid, effective, and low-cost geophysical method (Logachev and Zakharov 1973; Telford et al. 1990; Parasnis 1997; Eppelbaum and Khesin 2012). The accuracy of high-precision magnetic investigations may be 0.2–0.1 nT, or even less. At the same time, magnetic observations are notoriously complicated by numerous factors; the most common forms of noise affecting the magnetic investigations are discussed in the next section.

The complicated conditions of a magnetic survey require advanced methods of quantitative interpretation and 3-D modeling of magnetic anomalies (Khesin et al. 1996; Eppelbaum and Khesin 2012). The end product of a magnetic field application is the development of a corresponding physical–geological model (PGM) of the studied targets (Khesin et al. 1996).

One of the most important stages in the magnetic data examination is the quantitative analysis of magnetic anomalies (Fig. 1). Obviously, the first methodology of the quantitative interpretation of magnetic anomalies produced by thick bodies was published by Peters (1949). Among other studies carried out in this direction, those by Pyatnitsky (1961), Reford and Sumner (1964), Dukhovsky et al. (1970), Am (1972), Logachev and Zakharov (1973), Tafeyev and Sokolov (1981), Rao and Babu (1984), Ravat and Taylor (1998), and Flanagan and Bain (2013) may be noted. A quantitative

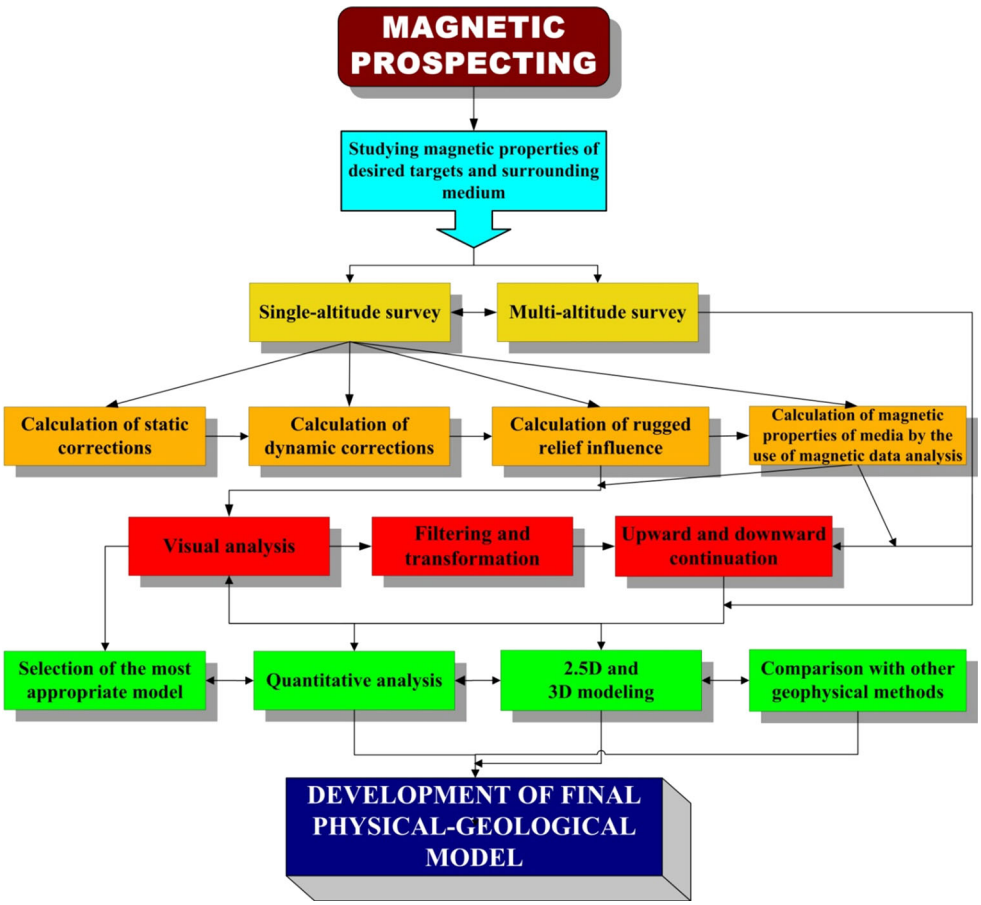

Fig. 1 Generalized block scheme of magnetic data processing and interpretation

analysis of magnetic anomalies from models of thin beds and horizontal circular cylinders (spheres) under complex environments was given in detail in Khesin et al. (1996) and Eppelbaum et al. (2001). Here, we present an interpretation of magnetic anomalies produced by thick beds, thin horizontal plates and intermediate interpreting models.

Noise in magnetic prospecting: a brief review

Magnetic surveys of potential archeological sites in Israel and in many other regions of the world are complicated by several kinds of noise (Eppelbaum and Khesin 2001; Eppelbaum et al. 2010; Eppelbaum 2011) (Fig. 2). These disturbances are briefly considered below.

Artificial (man-made) noise

The *industrial component* of noise mainly arises from power lines, cables, and various underground and transportation systems. The *instrumental component* is associated with the technical properties of magnetometers and their spatial locations, and *human errors*, obviously, can accompany geophysical observations at any time. Finally, *undocumented* (*poorly documented*) results of previous surveys can distort preliminary PGM development.

Natural disturbances

Nonstationary noise includes diurnal (time) variations, mainly from distant ionosphere disturbances. In the presence of strongly magnetized objects, these time variations can produce *secondary transient effects*. *Meteorological conditions* (rain, lightning, snow, hurricanes, etc.), and water movement in *basins and rivers* may also affect readings. *Soil–vegetation factors* associated with certain soil types (e.g., *swampy soil* or *loose ground* in deserts) and *dense vegetation*, which sometimes hampers movement along the profile, also need to be taken into account.

Geological–geophysical and archeological factors

These constitute the most important *geological–geophysical disturbances*. The application of any geophysical method depends primarily upon the existence of physical property differences between the objects under study and the surrounding medium. *The physical limitations* of the

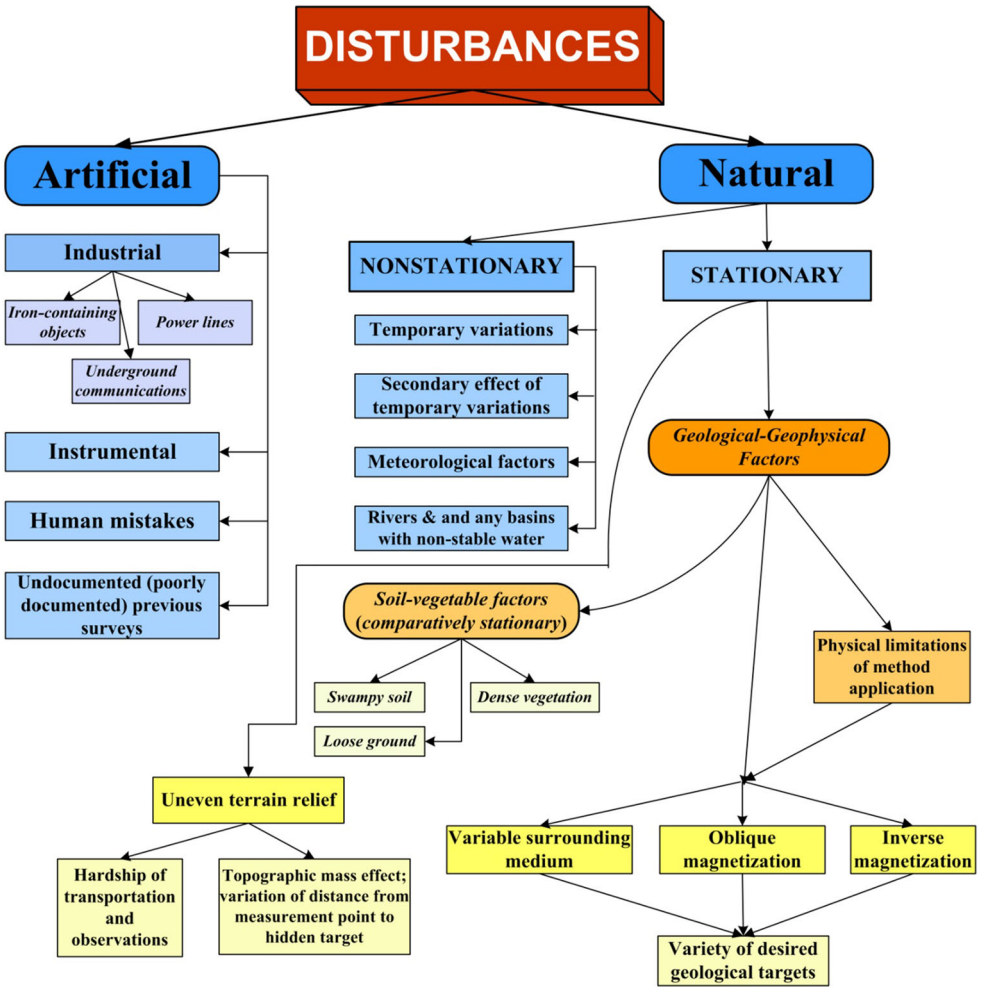

Fig. 2 *Block* scheme of disturbances appearing in the magnetometric investigations

methods reflect measurable magnetic and paleomagnetic contrast properties between the archeological targets and the geo-environmental sequence. *Uneven terrain relief* may negatively affect equipment transportation and magnetic data acquisition. Physically, this disturbance is generally twofold for potential and quasi-potential fields and involves the form and physical properties of the topographic features of the terrain relief as well as the effect of variations in the distance from the point of measurement to the hidden target (Eppelbaum et al. 2011).

Ancient earthquake damage is widely identified in many regions of the world. *The variety of anomalous sources* is composed of two factors: the variable surrounding medium, and the variety of archeological targets; both factors are crucial and greatly complicate the interpretation of magnetic data.

Oblique magnetization

Oblique magnetization disturbs these geophysical fields in the following way: the major extremum is shifted from the projection of the upper edge of the object in plan view, and an additional extremum may appear. An oblique magnetization is a characteristic particularity in most areas of the world.

Methodology of magnetic data quantitative interpretation over the thick bed model

There is no doubt that methodologies such as singular points (Troshkov and Groznova 1985); the Euler deconvolution method (e.g., Reid et al. 1990; Davis et al. 2010; Beiki 2013; Florio and Fedi 2014; Fregoso et al. 2015); analytical signal (e.g., Nabighian 1972; Roest et al. 1992); wavelet transform (e.g., Moreau et al. 1999; Vallée et al. 2004); various transformation methodologies (e.g., Salem et al. 2005; Chianese and Lapenna 2007; Phillips et al. 2007; Stampolidis and Tsokas 2012; Ialongo et al. 2014); and other similar procedures are rapid and effective methods. However, they often do not allow calculating such medium peculiarities as oblique magnetization (which may be different for various geological targets occurring in the area under study) and rugged terrain relief, and in many

cases they provide only some averaged information. For instance, in conditions of oblique magnetization, the "reduction to pole" procedure is often used—the calculation of pseudogravimetric anomalies (Blakely 1995). However, the procedure is suitable only when all interfering bodies in the studied area are magnetized parallel to the geomagnetic field and simultaneously when the bodies have subvertical dipping. Only in this case, the magnetic field can be recalculated correctly; the graphs obtained would be symmetrical, and further interpretation using conventional methods can be carried out.

Troshkov and Groznova (1985) have emphasized that magnetic field processing and interpretation is a highly complex physical–mathematical natural experiment where many disturbances usually occur. The author of this paper strongly supports this assertion. The methodology proposed here (see below) is based on the concept of separate (and detailed) examination of each identified anomaly. Nevertheless, application of the known automated methodologies (Euler deconvolution, analytic signal, etc.) in simple geological situations (vertical or subvertical magnetization vector location, flat relief, and quasi-uniform geological media) is more justified. A possible integration of these automatic methodologies with the method presented here may be an effective one, and further elaboration of this method envisages its formalization (tangents, intervals, etc.) and total automation.

The four most commonly used models in magnetic prospecting are (1) thin bed, (2a) horizontal circular cylinder (HCC), (2b) sphere, (3) thick bed, and (4) thin horizontal plate (Fig. 3). The methodology of magnetic anomalies' quantitative analysis in complex environments (oblique magnetization, rugged terrain relief and unknown level of the normal magnetic field) for models (1), (2a), and (2b) has been presented in several publications (Khesin et al. 1996; Eppelbaum et al. 2001; Eppelbaum and Mishne 2011). Several typical approximations of geological objects by models of the four classes are presented in Table 1.

Some common methodological questions concerning the thick bed model were noted in Khesin et al. (1996). First of all, it is necessary to point out that all interpretation methods developed for the vertical component Z (ΔZ) can be applied for the analysis of the total magnetic field T (ΔT). Let us consider the interpretation methodology:

(1) Effective magnetic moment M_e. Generally speaking, it is an effective magnetic moment of its volume unit for an inclined thick bed, i.e., effective magnetization (M_e^v). The expression for the Z anomaly is

$$M_e^v = J_e \sin(\phi_2 - \phi_1), \quad (1)$$

where $J_e = JC_m$ is the effective body magnetization (for ΔT anomalies, value C_m is replaced by C_mC_0); φ_1 is the angle of inclination for the upper edge of a thick bed; φ_2 is the inclination of lateral boundaries of a thick bed; $C_m = \sin i_m / \sin \phi_m$, i_m is the inclination of the thick bed magnetization vector **J** to the horizon; φ_m is the inclination angle of the magnetization vector projection on the vertical plane of the profile; $C_0 = \sin i_0 / \sin \phi_o$; i_0 is the geomagnetic inclination (a common inclination in the area under study); and ϕ_0 is the projection of the local geomagnetic inclination direction onto the vertical plane oriented in the direction of the profile (see also Table 2).

(2) The generalized angle θ (reflecting the degree of magnetic anomaly asymmetry as a functional relation of the anomalous body geometric form, value of magnetization, magnetic inclination, and observation profile azimuth) for the Z anomaly is determined as in Khesin et al. (1996)

$$\theta = \gamma_m - \gamma_2 + \phi_1, \quad (2)$$

where $\gamma_2 = 90^o - \phi_2$ and $\gamma_m = 90^o - \phi_m$. For the ΔT anomaly, γ_m should be replaced by $\gamma_o + \gamma_m$, where $\gamma_0 = 90^o - \phi_0$ (angle completing the geomagnetic inclination to the vertical in the profile plane).

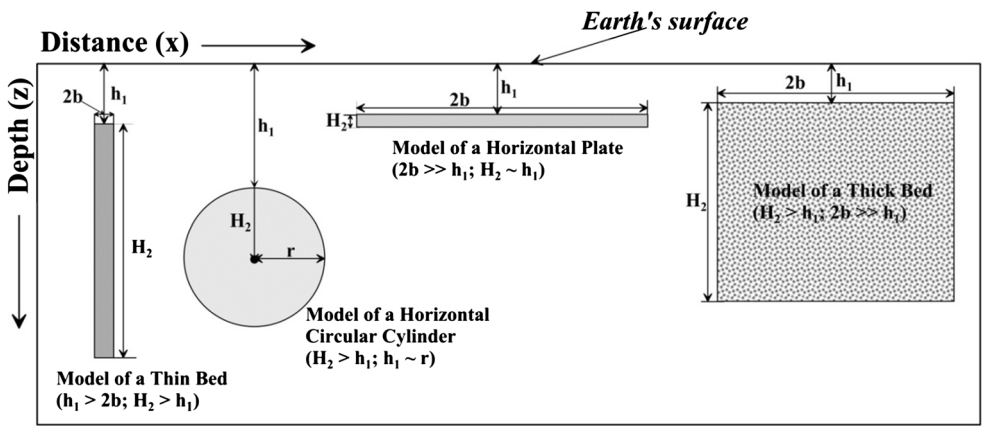

Fig. 3 Main models of anomalous bodies used in magnetic anomaly analysis

Table 1 Typical approximation of geological objects by bodies of the simplest shape (according to Eppelbaum and Khesin (2012), revised and supplemented)

Geological–geophysical targets		Approximation
Objects outcropping onto the Earth's surface and under overburden	Buried or cropping out when surveying aerially	
Tectonic–magmatic zones, sill-shaped intrusions and thick dikes, large fault zones, thick sheet-like ore deposits, salt bodies	Tectonic–magmatic zones, thick sheet intrusions and zones of hydrothermal alterations	Thick bed
Thin dikes, zones of disjunctive dislocations and hydrothermal alterations, sheet-like ore deposits, veins	Sheet intrusions, dikes, disjunctive dislocations, sheet-like ore deposits	Thin bed
Lens- and string-like deposits	Folded structures, elongated morphostructures, large mineral lenses	Horizontal circular cylinder
Pipes, vents of eruption, ore shoots	Intrusions (isometric in plane), pipes, vents of volcanoes, large ore shoots	Vertical and (inclined) circular cylinder or pivot
Karst cavities, ore bodies	Brachy-anticlines, brachy-synclines, isometric morphostructures, karst terranes, hysterogenetic ore bodies	Sphere
Traps, thin basaltic layers, salt layers	Intrusions, evaporites	Thin horizontal plate

Table 2 Variables applied for quantitative analysis of ΔT anomalies due to model of obliquely magnetized thick bed

Variable	Description
M_e^v	Effective magnetization
$\mathbf{J}$	Magnetization vector
J_e	Effective body magnetization
φ_1	Angle of inclination for the upper edge of a thick bed
φ_2	Inclination of lateral boundaries of a thick bed
θ	Generalized angle reflecting the degree of magnetic anomaly asymmetry as a function relation of an anomalous body geometric form, value of magnetization, magnetic inclination and observation profile azimuth
i_m	Inclination of the thick bed magnetization vector $\mathbf{J}$ to the horizon
φ_m	Inclination angle of the magnetization vector projection on the vertical plane of the profile
i_0	Geomagnetic inclination (a common inclination in the area under study)
$2b$	Horizontal thickness (size) of a thick bed
ϕ_0	Projection of the local geomagnetic inclination direction onto the vertical plane oriented in the direction of the profile
(x_1, h_1^1)	Coordinate of first angular point of the inclined thick bed upper edge
(x_2, h_1^2)	Coordinate of second angular point of the inclined thick bed upper edge
$h = \frac{h_1+h_2}{2}$	Average depth to the upper edge
$l = 0.5(h_1^2 - h_1^1)$	Half of the vertical distance between the angle points of the thick bed's upper edge
k_θ	$\frac{d_8}{d_4}$
β	Relative half-thickness $= \frac{b}{h}$
k_m	Anomaly amplitude by $h = 1$, $2M_e = 1$, and specified values θ and β
k_0	$k_0 = \frac{\lvert Z_{min}\rvert}{Z_{max}}$, but when $\theta = 0$, $k_0 = \frac{Z_l}{Z_{max}}$

(3) Coordinates of angular points $(x_1, h_1^1)$and (x_2, h_1^2) (here $(x_2 - x_1) = 2b$ is the horizontal thickness of the thick bed model).

(4) Abscissa of the epicenter (projection onto the plan view of the mid-point of the upper edges of the thick bed), which does not coincide with the abscissa of the anomaly maximum (or minimum) of anomaly, due to the effect of oblique magnetization.

Localization of the epicenter and determination of the generalized angle θ are specific features of magnetic anomaly interpretation under the oblique magnetization effect. The other interpretation problem is the determination of the normal background level (ΔZ_{backgr} or ΔT_{backgr}) for the anomalies under study.

For the techniques described below, the angle θ is understood to be in the range of 0°–90°, the Ox-axis is oriented to the north (to the right in the figures), and the Oz-axis oriented downward.

Improved characteristic point method

The case of a thick bed fails to yield applicable analytical expressions for the relations between the bed's parameters and characteristic points. The bed's central point can be defined by the analysis of the horizontal gradient Z_x:

$$Z_x = \frac{\partial Z}{\partial x} = M_e \left[\frac{(h-l)\cos\theta - (x+b)\sin\theta}{(x+b)^2 + (h-l)^2} - \frac{(h+l)\cos\theta - (x-b)\sin\theta}{(x-b)^2 + (h+l)^2} \right].$$

where $h = 0.5(h_1^1 + h_1^2)$ is the average depth of a thick bed with the inclined upper edge (Fig. 4), $l = 0.5(h_1^2 - h_1^1)$, i.e., half of the vertical distance between the angle points of the thick bed's upper edge (Fig. 4).

The greatest extremes of the Z_x curve have the following abscissae (Khesin et al. 1996):

$$x_l = -b - (h-l)\frac{1-\cos\theta}{\sin\theta},\ x_r = b - (h+l)\frac{1-\cos\theta}{\sin\theta}. \quad (3)$$

From Eq. (3), it follows that both left and right inflection points are distorted along the profile to the south (Ox-axis is north oriented) from projections of the thick bed's angle points to the surface (Fig. 4). When $\theta = 0$, the inflection points are not distorted; when $\theta = 90$, the distortion is greatest: $h - l$ for the left point and $h + l$ for the right. Thus, by any θ (in the interval 0–90°), the inflection points of magnetic anomaly produced by a thick bed occur in the vicinity of its angle point, with some distortion to the south.

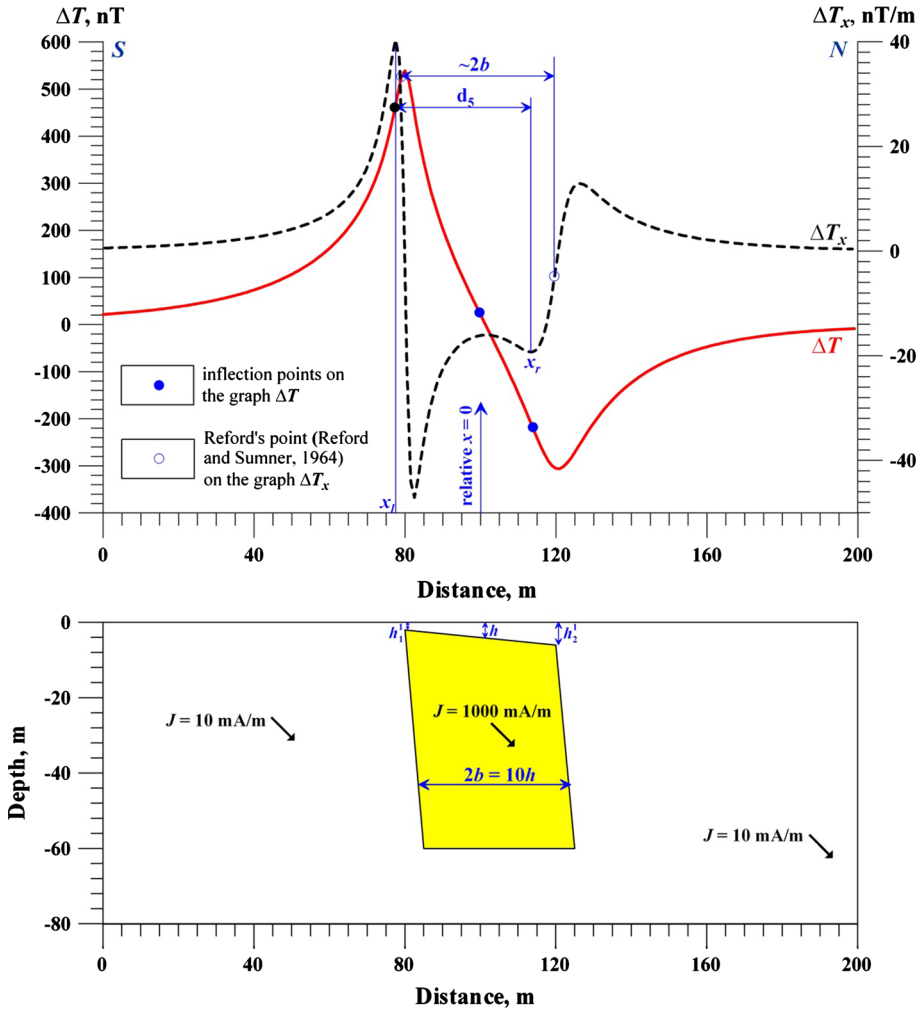

Fig. 4 Location of characteristic points on graphs ΔT and its horizontal gradient ΔT_x from the obliquely magnetized thick bed ($2b \gg h$) with inclined *upper edge*. J is the magnetization vector)

The approximate horizontal thickness of the thick bed may be determined from the distance between the inflection points d_5:

$$d_5 = x_r - x_l = 2b - \left(h_1^2 - h_1^1\right)\frac{1-\cos\theta}{\sin\theta} = 2b\left(1 - \tan\phi_1 \tan\frac{\theta}{2}\right). \quad (4)$$

If $2b \gg h$, it is possible to obtain the exact position of the thick bed lateral faces in the plane by Reford's point (Reford and Sumner 1964) determined on each pulse of the obtained curve Z_x. The distance between these points equals the bed thickness (within the bounds of the gradient determination accuracy), and the point of origin occurs at the mid-point between these pulses. It is possible to interpret the above-mentioned pulses of the curve Z_x by the available formulas for a thin bed (the methodology of magnetic anomaly interpretation over a model of thin bed was given earlier in Eppelbaum et al. (2001)).

If $h_1 = h_2$ (upper edge is horizontal), the parameters of the thick bed may be found in the following way: if we determine the central point by the above-mentioned method or by the tangent method (see below), it will be easy to select Z symmetrical and asymmetrical parts from the graph:

$$\left\{\begin{array}{l} Z_{vv}(x)\cos\theta = 0.5[Z(x) + Z(-x)], \\ X_{vv}(x)\sin\theta = 0.5[Z(x) - Z(-x)]. \end{array}\right\}.$$

Using the known characteristic point methods ($x_{0.5}$, $x_{0.25}$) (Logachev and Zakharov 1973; Telford et al. 1990) on the curve $Z_{vv}\cos\theta$ will enable finding parameters h and b. To determine values for M_e and θ, both Z_{vv} and X_{vv} curves may be used. To do this, the data presented in Table 3 are applied, where using the value of $\beta = {}^{b}/_{h}$ by $\theta = 0$ and $\theta = 90^{o}$ will enable finding two values of coefficient k_m (k_m is the anomaly amplitude by $h = 1$, $2M_e = 1$, and specified values θ and β)—k_{m0} and k_{m90}. Then, the $M_e = Z_A/2k_m$ equation is applied to determine $M_e\cos\theta$ by Z_{vv} and $M_e\sin\theta$ by X_{vv}. The values obtained are finally used to find M_e and θ.

It should be noted that the characteristic point method usually plays a secondary role to the tangent method (see below).

Improved tangent method

Unlike the method of characteristic points, the tangent method uses not only x and y coordinates of maximum and minimum points, and inflection points and their differences, but also the first horizontal derivative in inflection points (where the first derivative has its extrema) (Fig. 5). These values can be readily obtained from the anomaly plot as tangents of the inclination angles of the tangents to the curves at the inflection points. This, along with the acceptable accuracy of the method, favors an effective application of it. This PGM, as well as models presented in Figs. 6, 7, 8, 9, was computed using developed GSFC-M [Geological Space Field Computation, Modified (Khesin et al. 1996; Eppelbaum 2006)] software intended for combined 3-D modeling of magnetic and gravity fields in complex environments.

A somewhat different variant of the tangent method was suggested by Peters (1949). Quite a number of modifications of the tangent method are available today (Pyatnitsky 1961; Reford and Sumner 1964; Dukhovsky et al. 1970; Tafeyev and Sokolov 1981; Rao and Babu 1984, and others). However, there is really no methodology intended for reducing the inclined magnetization effect and determining θ (which is an important parameter of the obliquely magnetized anomalous bodies) as well as methodologies applicable in conditions of rugged terrain relief and complex host media.

The modification discussed below is designed especially for the conditions of oblique magnetization and inclined relief. This technique enables us to determine θ and to

Table 3 Values of computed coefficients k_m and k_0

Parameter θ, degree	Parameter β							
	0.1	0.5	1	2	3	5	8	10
k_m								
0	0.199	0.927	1.571	2.214	2.498	2.747	2.893	2.942
30	0.200	0.936	1.623	2.416	2.865	3.404	3.886	4.112
60	0.200	0.954	1.718	2.745	3.410	4.274	5.081	5.446
90	0.200	0.962	1.763	2.887	3.637	4.625	5.553	5.996
k_0								
0	0.000	0.000	0.000	0.000	0.000	0.000	0.000	0.000
30	0.073	0.076	0.088	0.115	0.140	0.177	0.216	0.234
60	0.334	0.346	0.372	0.425	0.464	0.496	0.557	0.576
90	1.000	1.000	1.000	1.000	1.000	1.000	1.000	1.000

Parameters β, k_m and k_0 are explained in the text (see section on "Improved tangent method") and in Table 2

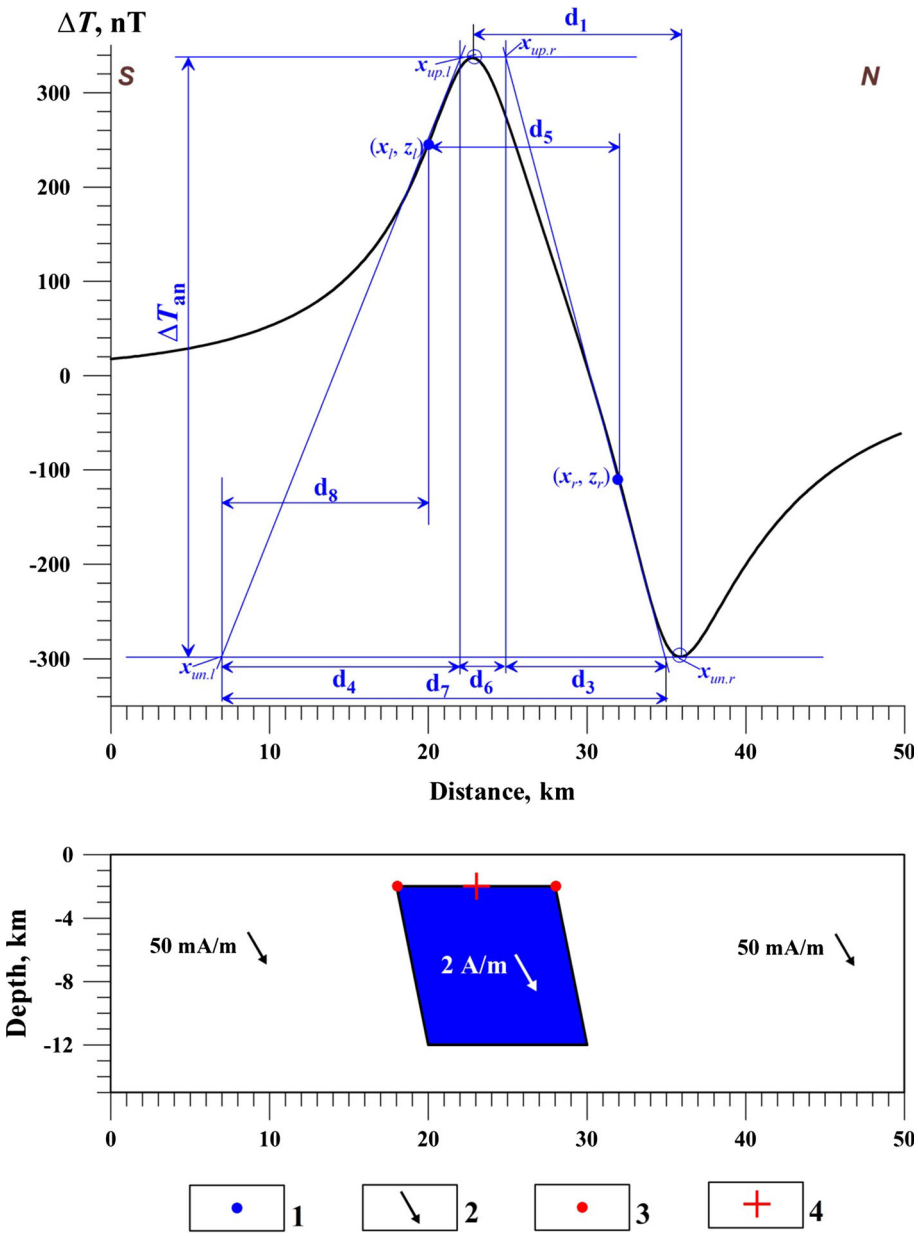

Fig. 5 Tangents and characteristic segments used for the interpretation of a ΔT anomaly caused by an obliquely magnetized thick bed situated in a non-magnetic medium. *1* inflection points of the ΔT anomaly plot, *2* position of the magnetization vector, *3* position of left and right angular points of the thick bed, *4* position of the middle of the thick bed *upper edge*. *Tangents* 1,2—*left-hand* and *right-hand* inclined ones, respectively, 3,4—*upper and lower horizontal ones*, respectively. Locations of intervals d_1–d_8 are explained in the text (see section on "Improved tangent method")

localize the point of origin (i.e., position of the body's epicenter) in the course of the interpretation. Four tangents are used: two inclined ones, passing through the inflection points with the largest in absolute values of horizontal field gradient, and two horizontal ones, passing through the maximum and the largest absolute minimum of the anomaly (Fig. 5).

The inflection points at the inclined tangents are closest to the largest in absolute value extrema of the anomaly and are found to their left for θ changing from 0 to 90° and the axis Ox running approximately to the north (to the right in the figures).

For a thick bed with a horizontal upper edge, besides the segment d_5 [see Eq. (4)] and $d_1 = x_{\min} - x_{\max}$, parameters d_3, d_4, d_6, d_7 and d_8 can be calculated by the following proportions (Fig. 5):

$$\left\{ \begin{array}{l} d_3 = x_{\text{un.r}} - x_{\text{up.r}}, \\ d_4 = x_{\text{up.l}} - x_{\text{un.l}}. \end{array} \right\}. \tag{5}$$

The following segments are also used (Fig. 5):

$$\left\{ \begin{array}{l} d_6 = x_{\text{up.r}} - x_{\text{up.l}}, \\ d_8 = x_l - x_{\text{un.l}}. \end{array} \right\}. \tag{6}$$

It is obvious that $d_7 = d_3 + d_4 + d_6$.

Here, $x_{\text{up.r}}$, $x_{\text{un.r}}$, $x_{\text{up.l}}$, $x_{\text{un.l}}$ are, respectively, the x coordinates of the upper right, lower right, upper left and

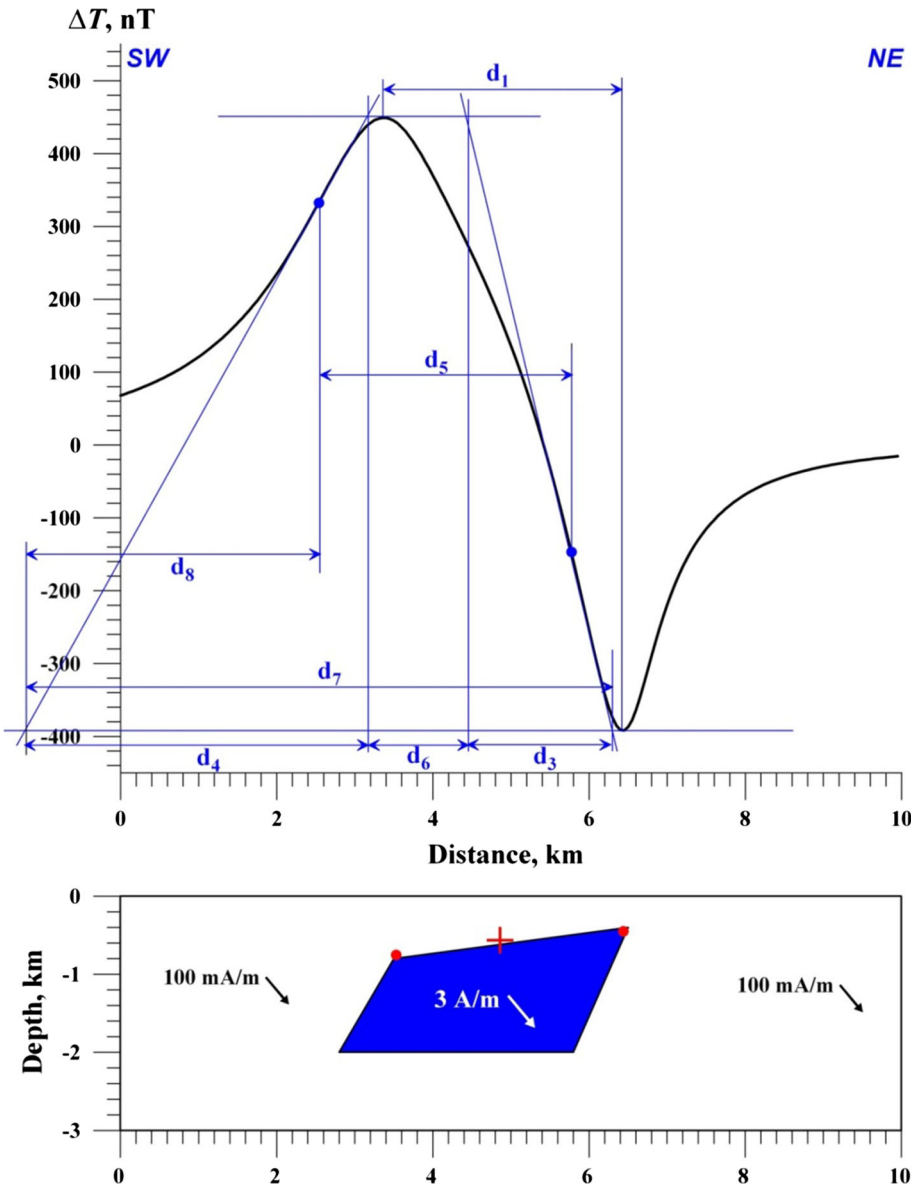

Fig. 6 Quantitative analysis of magnetic field from a model of ancient limestone wall. Crossing designates the position of the middle of the *upper edge* of the thick bed, and *bold points* designate the position of the *eft-hand* and *right-hand* angular points of the target

lower left points of intersection of the inclined tangents with the horizontal ones:

$$\left\{\begin{array}{l} x_{\text{up.r}} = x_r - \dfrac{Z_{\max} - Z_r}{|Z_{\text{xr}}|}, \\ x_{\text{un.r}} = x_r - \dfrac{Z_r - Z_{\min}}{|Z_{\text{xr}}|} \end{array}\right\}. \tag{7}$$

$$\left\{\begin{array}{l} x_{\text{up.l}} = x_l + \dfrac{Z_{\max} - Z_l}{|Z_{\text{xl}}|}, \\ x_{\text{un.l}} = x_l - \dfrac{Z_l - Z_{\min}}{|Z_{\text{xl}}|} \end{array}\right\}. \tag{8}$$

Z_{xr} and Z_{lr} are the right and left tangents, respectively, applied to curve Z, and x_r and x_l values are determined from the equation

$$\frac{\partial^2 Z}{\partial x^2} = 0, \tag{9a}$$

and $Z_{\max}$ and $Z_{\min}$ values are obtained from the equation

$$\frac{\partial Z}{\partial x} = 0. \tag{9b}$$

Equation (9a) has from 2 to 5 real roots, depending on values θ and β (relative half-thickness $\beta = b/h$) and cannot be solved in a general form. Therefore, it was solved using the well-known Newton–Raphson numerical method (e.g., Stroud 2001), with θ equal to 15, 30, 45, 60, 75° and β equal to 0.1, 0.5, 1, 1.5, 2, 3, 5, 8, 10.

The values of Z_r, Z_l, Z_{xr} and Z_{xl} were calculated by the obtained values of x_r and x_l. After this, left-hand sides of

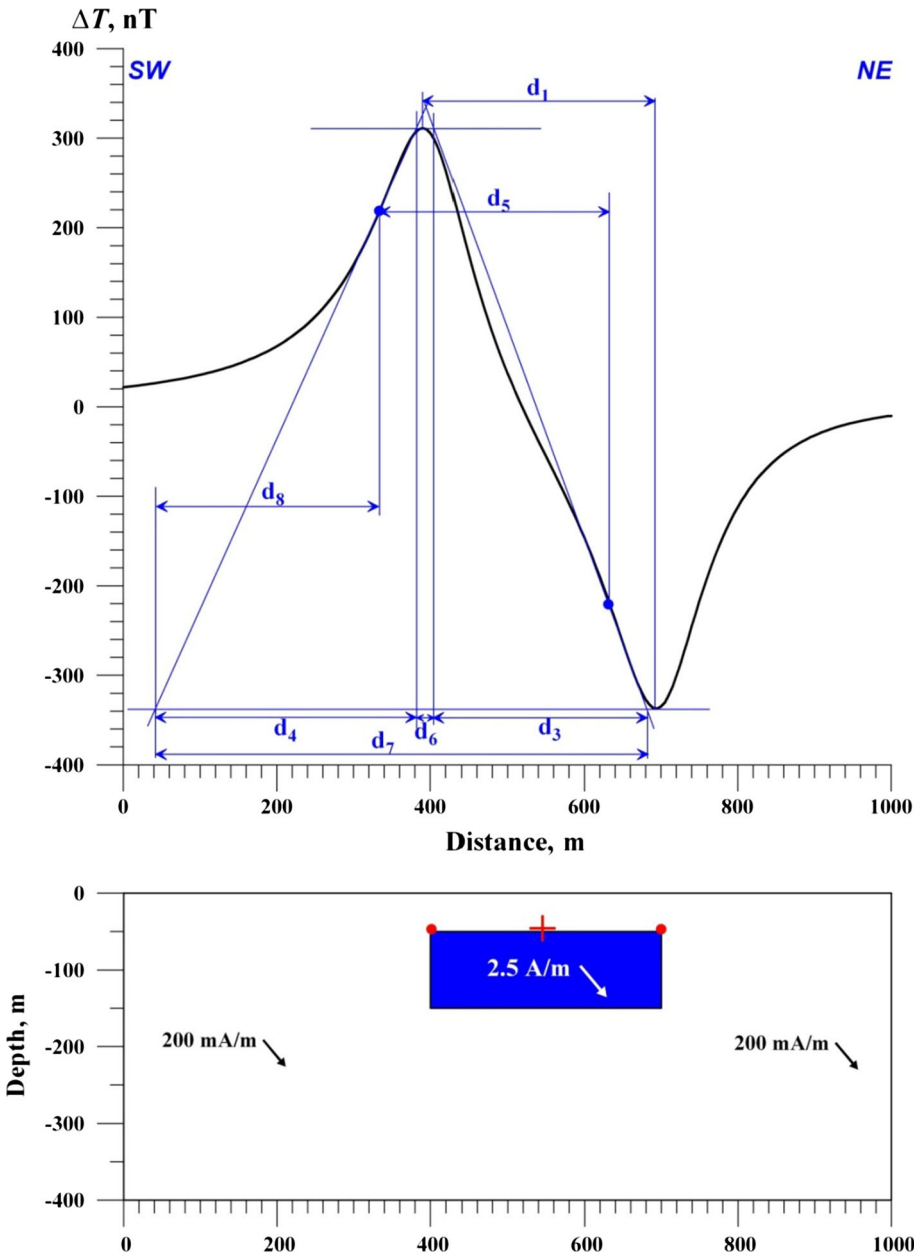

Fig. 7 Example of quantitative analysis of magnetic field from the object occupying intermediate position between the model of thick bed and *thin horizontal* plate

Eqs. (5), (6), (7), and (8) were obtained. In the computations, it was assumed that $h = 1$, $2M_e = 1$, $b = \beta$. The values obtained are denoted by a tilde ("$\sim$"), and the values of d_3, d_4, d_6 and d_8 for $h = 1$ are denoted by k_3, k_4, k_6 and k_8, respectively.

The desired values in the R.H. sides of Eqs. (5), (6), (7), and (8) are calculated for θ equaling 15, 30, 45, 60, 75° and β equaling 0.1, 0.5, 1, 1.5, 2, 3, 5, 8, 10. It is assumed that $h = 1$, $2M_e = 1$, $b = \beta$. The values obtained are denoted by a tilde, and the values of d_3, d_4, d_6 and d_8 for $h = 1$ are denoted by k_3, k_4, k_6 and k_8, respectively.

Table 4 presents the $k_\theta = f(\theta)$, $k_{\beta\theta} = f_1(\theta, \beta)$ and $k'_{\beta\theta} = f_2(\theta, \beta)$ relationships, where

$$k_\theta = \frac{k_8}{k_4} = \frac{d_8}{d_4}, \tag{10}$$

$$k_{\beta\theta} = \frac{k_3}{k_4} = \frac{d_3}{d_4}, \tag{11}$$

$$k'_{\beta\theta} = \frac{k_4}{k_6 + k_3} = \frac{d_4}{d_6 + d_3}. \tag{12}$$

Table 4 enables calculating θ from k_θ and the half-thickness β by the obtained θ, using $k_{\beta\theta}$ and $k'_{\beta\theta}$ determined from graph ΔZ (ΔT). The need to use $k'_{\beta\theta}$ along with $k_{\beta\theta}$ can be explained by the fact that the β value obtained from $k_{\beta\theta}$ for small θ is not reliable.

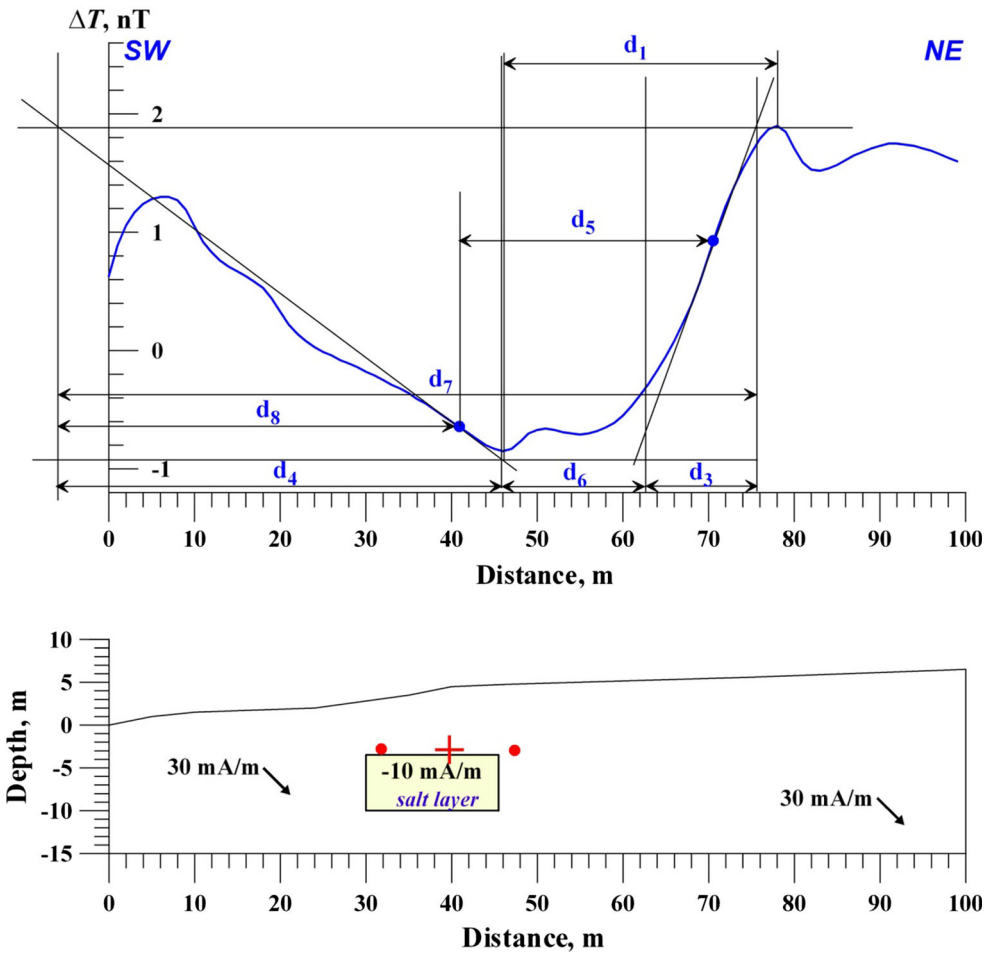

Fig. 8 Quantitative analysis of magnetic anomaly over the model of salt thick bed computed for the conditions of rugged terrain relief

Table 5 helps to determine k_3, k_4 and k_6 by the obtained values of θ and β. One way to obtain values $\tilde{x}_{\text{un.r}}$ and $\tilde{x}_{\text{un.l}}$ and k_{m} ($k_{\text{m}} = \Delta Z$ (ΔT_{an}) when $h = 1$, $2M_{\text{e}} = 1$) and $k_0 = \frac{|Z_{\min}|}{Z_{\max}}$ (when $\theta = 0$, $k_0 = \frac{Z_l}{Z_{\max}}$) is shown in Table 6.

The following shows how the interpretation is carried out (modified from Khesin et al. 1996):

(1) Determination of θ and the relative half-thickness β. The necessary tangents to the anomaly curve are plotted (see Fig. 5), and the segments d_3, d_4, d_6, d_8, T_{A} (T_{A} is the amplitude of anomaly ΔT) are determined from the magnetic anomaly graph. The coefficients k_θ, $k_{\beta\theta}$ and $k'_{\beta\theta}$ are calculated by Eqs. (10)–(12). Then, with θ obtained from k_θ from Table 4, two values of β are obtained from $k_{\beta\theta}$ and $k'_{\beta\theta}$ and averaged, if they are close.

(2) Determination of the depth h of the bed upper edge. The coefficients k_3, k_4 and k_6 obtained from θ and β are presented in Table 5. The depth h is calculated using the equation $h_i = \frac{d_i}{k_i}$, where d_i is a characteristic segment and k_i is a coefficient corresponding to this segment. Then, an average value $h_{\text{aver}} = \frac{h_1+h_2+h_3}{3}$ is obtained.

(3) Determination of half of the horizontal thickness b is by the formula

$$b = \beta h. \tag{13}$$

(4) Determination of the effective magnetic moment M_{e} is by the formula

$$M_{\text{e}} = \frac{T_{\text{A}}}{2k_{\text{m}}}. \tag{14}$$

The coefficient k_{m} is obtained from the known values of θ and β in Table 5.

(5) Localization of the epicenter (the origin of coordinates). This operation is performed using $x_{\text{un.r}}$ and $x_{\text{un.l}}$, which are calculated by the formulas

$$\left\{ \begin{array}{l} x_{\text{un.r}} = h\tilde{x}_{\text{un.r}} \\ x_{\text{un.l}} = h\tilde{x}_{\text{un.l}} \end{array} \right\}, \tag{15}$$

where $\tilde{x}_{\text{un.r}}$ and $\tilde{x}_{\text{un.l}}$ are obtained from the known values of θ and β in Table 6.

The segments $x_{\text{un.r}}$ and $x_{\text{un.l}}$ are plotted from the corresponding points of intersection of the inclined tangents and

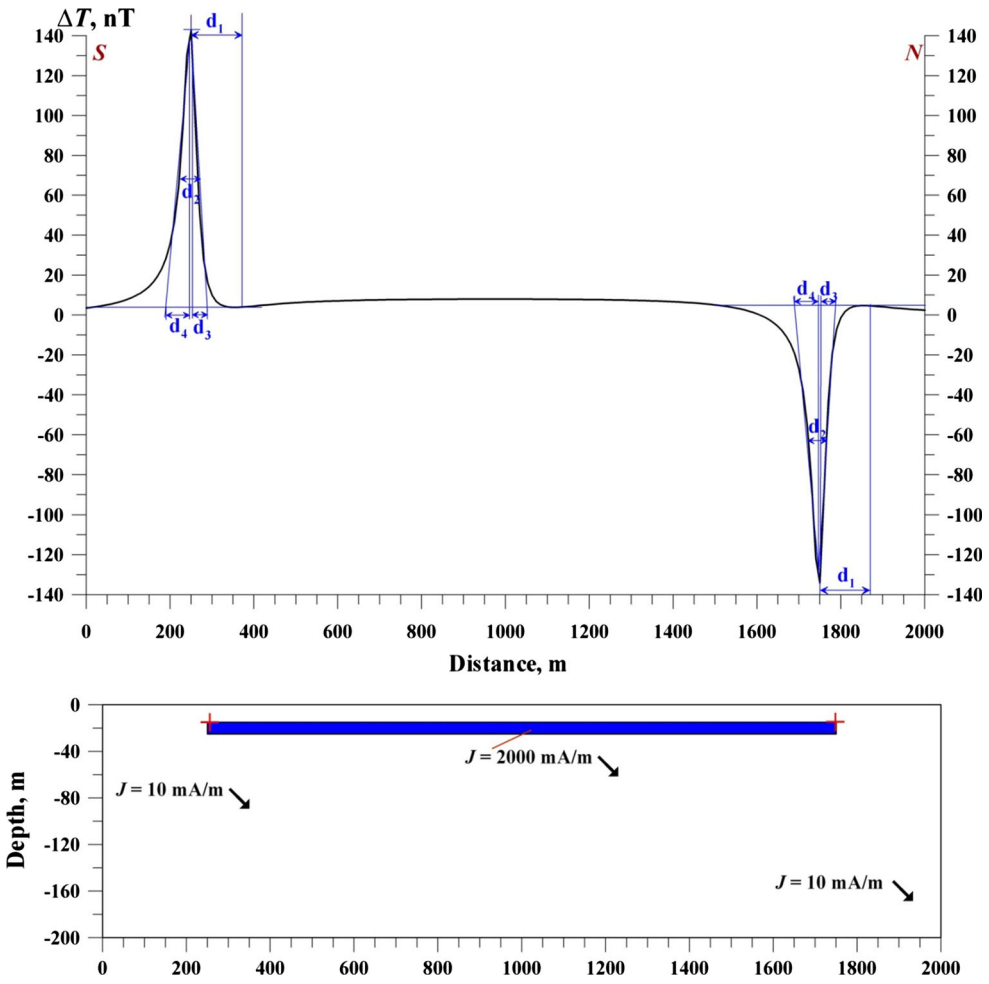

Fig. 9 Quantitative analysis of magnetic anomalies produced by a classic thin plate ($2b \gg h_1$ and h_2, and vertical thickness of the thin plate (h_2-h_1) is compatible with h_1). *Symbol* + designates position of the center of *upper edge* of fictitious thin beds

the lower horizontal one. The mid-point between the ends of these segments defines the epicenter location.

(6) Determination of the correction ΔT_{backgr} in the normal background level:

$$\Delta T_{\text{backgr}} = \Delta T_{\min} + \Delta T \frac{k_0}{1 + k_0}. \quad (16)$$

The value of $k_0 = \frac{|\Delta T_{\min}|}{|\Delta T_{\max}|}$ is obtained from Table 3.

This modification has been tested on typical (theoretical) curves of ΔT anomalies due to a depth-limited thick bed with θ equal to 0, 30, 60 and 90°, $\beta = 1$–10. This suggests that the version just discussed is theoretically accurate.

The modification tested for thick beds with unlimited lower edges has shown the good accuracy of Q, h_1, b and M_e determination (2–3° forθ, 3–4 % for h and b, 2 % for M_e).

This modification has also been tested on typical curves of ΔT due to the oblique $\varphi_2 = (45, 60, 90, 120^\circ)$ inductively magnetized ($i_m = 45^\circ$) (this direction of magnetization is a typical average for the Eastern Mediterranean region) beds of a variable thickness ($\beta = 1$–4), with the lower edge at the depth of h_2 (h_2/h_1 = unlimited, 6 and 3) (Table 7). The results prove that the modification can be applied for interpreting anomalies caused by depth-limited beds. In fact, the errors in the parameter determination for depth-limited beds tend to increase in comparison with the case of depth-unlimited beds. Still, they are acceptable in a practical way (max. 15–20 %).

It should be noted that sometimes a combination of characteristic point and tangent methods may give maximal interpretation reliability. For improving the magnetic data resolution, the distance between the observation points in anomalous areas must be condensed. In addition, the comparison of magnetic observations carried out at two levels may provide valuable information about the hidden targets.

Our experience (Khesin et al. 1996; Eppelbaum et al. 2001; Eppelbaum 2011; Eppelbaum and Khesin 2012) indicates that the anomalous part of the magnetic graph must be described by at least 15–18 points (over complex geological sections, the more dense observation set may be necessary).

Table 4 Values of computed coefficients k_θ, $k_{\beta\theta}$ and $k'_{\beta\theta}$

parameter θ, degree	parameter β							
	0.1	0.5	1	2	3	5	8	10
k_θ								
0	0.749	0.714	0.667	0.594	0.561	0.536	0.521	0.517
30	0.820	0.810	0.793	0.783	0.784	0.795	0.810	0.817
60	0.833	0.881	0.880	0.884	0.889	0.900	0.908	0.913
90	0.934	0.935	0.933	0.935	0.939	0.941	0.947	0.950
$k_{\beta\theta}$								
0	1.0	1.0	1.0	1.0	1.0	1.0	1.0	1.0
30	0.544	0.578	0.656	0.774	0.840	0.899	0.935	0.948
60	0.280	0.314	0.403	0.580	0.687	0.796	0.866	0.891
90	0.126	0.148	0.207	0.382	0.520	0.672	0.799	0.819
$k'_{\beta\theta}$								
0	0.799	0.780	0.694	0.527	0.406	0.272	0.180	0.147
30	1.374	1.259	1.039	0.727	0.554	0.383	0.269	0.226
60	2.429	2.183	1.741	1.180	0.906	0.636	0.454	0.386
90	4.684	4.242	3.387	2.190	1.629	1.115	0.783	0.661

Table 5 Values of computed coefficients k_3, k_4 and k_6

Parameter θ, degree	Parameter β							
	0.1	0.5	1	2	3	5	8	10
k_3								
0	1.545	1.680	1.949	2.352	2.567	2.774	2.904	2.950
30	1.213	1.369	1.732	2.416	2.888	3.492	4.042	4.300
60	1.056	1.238	1.730	2.906	3.839	5.117	6.321	6.891
90	1.008	1.203	1.763	3.569	5.423	7.583	9.804	10.853
k_4								
0	1.545	1.680	1.949	2.352	2.567	2.774	2.904	2.950
30	2.233	2.367	2.640	3.120	3.436	3.883	4.321	4.537
60	3.773	3.937	4.294	5.012	5.588	6.432	7.299	7.733
90	8.003	8.156	8.512	9.344	10.092	11.283	12.580	13.252
k_6								
0	0.389	0.472	0.850	2.113	3.755	7.423	13.220	17.150
30	0.412	0.511	0.809	1.875	3.312	6.644	12.033	15.671
60	0.498	0.565	0.737	1.343	2.332	4.987	9.745	13.162
90	0.701	0.720	0.751	0.699	0.951	2.537	6.272	9.208

Disturbing effects of an inclined profile

If anomalies are observed on an inclined profile, then the parameters obtained characterize a certain fictitious body. The transition from fictitious body parameters to those of the real body is performed using the following expressions (the subscript "r" stands for a parameter of the real body) (Khesin et al. 1996)

$$\left\{\begin{array}{l} h_r = h + x\tan\omega_0, \\ x_r = -h\tan\omega_0 + x_0, \end{array}\right\}, \qquad (17)$$

where h is the depth of the upper edge occurrence, x_0 is the location of the source's projection to plan view relative to the extremum having the greatest magnitude, and ω_0 is the angle of the terrain relief inclination ($\omega_0 > 0$ when the inclination is toward the positive direction of the x-axis).

Undoubtedly, all the above-mentioned procedures should be computerized and the role of the interpreter will be reduced to check (and possibly correcting) the automatically selected parameters in the magnetic curves.

Table 6 Values of computed coefficients $\tilde{x}_{un.r}$ and $\tilde{x}_{un.l}$

Parameter θ, degree	Parameter β							
	0.1	0.5	1	2	3	5	8	10
$\tilde{x}_{un.r}$								
0	1.740	1.916	2.374	3.408	4.445	6.486	9.514	11.525
30	1.180	1.338	1.730	2.683	3.664	5.658	8.627	10.622
60	0.793	0.928	1.281	2.214	3.191	5.167	8.151	10.146
90	0.504	0.602	0.881	1.789	2.774	4.747	7.730	9.722
$\tilde{x}_{un.l}$								
0	1.740	1.916	2.374	3.408	4.445	6.486	9.514	11.525
30	2.678	2.909	3.451	4.728	5.971	8.361	11.770	13.976
60	4.529	4.812	5.479	7.047	8.568	11.369	15.213	17.640
90	9.208	9.477	10.144	11.822	13.512	16.656	20.928	23.591

Table 7 Results of the improved tangent method testing on ΔT anomalies computed from the models of obliquely magnetized thick beds

Anomalous bodies (beds)	Determination error			
	θ, degree	h_1 (%)	b (%)	M_e (%)
Depth-unlimited	12	13	11	14
Depth-limited with $h_2/h_1 = 6$	15	14	15	18
Depth-limited with $h_2/h_1 = 3$	17	15	16	20

Possible determination of the lower edge of thick and "quasi-thick" bodies

Most reliably, the depth of a magnetized body's lower edge may be determined by the application of 3-D magnetic field modeling integrated with other geophysical and geological methods (e.g., Blakely 1995; Eppelbaum and Khesin 2012; Eppelbaum and Katz 2015).

In the regional magnetic data analysis, a maximum possible magnetized body lower edge occurrence may be calculated by estimating the Curie point depth (e.g., Pilchin and Eppelbaum 1997; Eppelbaum et al. 2014). Considering the estimation of the lower edge of the *depth-unlimited bodies* ($H_2/h_1 \geq 10$; explanation of these parameters is given in Fig. 3) (when the lower edge of magnetized body does not reach the depth of Curie point) is a complex geophysical–geological problem.

To estimate the lower edge for the *depth-limited body* characterized by $H_2/h_1 \leq 5-7$ various methodologies (e.g., Bulina 1970; Nikitsky and Glebovsky 1990; Khesin et al. 1996) were developed; the Bulina (1970) semi-empirical formula is one of the simplest:

$$H_2 = 2d_1 - 1.8h_1,$$

where parameter d_1 is presented in Fig. 5.

At the same time, Bulina's (1970) method does not calculate the effect of inclined magnetization and cannot be applied for the case when $h_1 \gg 2b$.

Application to models and field examples

Models

A preliminary testing of the quantitative interpretation method on the model of thick bed is shown in Fig. 5.

The PGM presented in Fig. 6 is typical of the Caucasus, Mediterranean, and many other regions of the world: a magnetic body ($J = 3000$ mA/m) having a form of thick bed (basalt) with an inclined upper edge and inclined lateral boundaries occurs in the low magnetized medium (100 mA/m). Applying the aforementioned interpretation methodology enabled determination of the position of the middle of the upper edge of the bed and left and right angular points of the upper edge with great accuracy. The calculation of magnetization J_e by the use of Eqs. (1) and (14) gives us the value of 2700 mA/m.

The next model (Fig. 7) is of the greatest interest. This PGM occupies an intermediate geometrical form between the thick bed and thin horizontal plate (as it is closer to the model of the thin plate). It is necessary to note that a thin horizontal plate model is difficult to analyze in conditions of oblique magnetization and unknown levels of the normal field (Logachev and Zakharov 1973; Telford et al. 1990). Applying the aforementioned methodology to interpret the magnetic anomaly due to this intermediate target enabled obtaining the parameters of the anomalous body with the required accuracy. This model is more complex, and the determined J_e value consisted of 2100 mA/m (the value assumed for the anomalous body in the PGM is 2500 mA/m against 200 mA/m of the host medium).

Figure 8 shows the quantitative analysis of a magnetic anomaly produced by a salt layer that may be approximated by the thick bed model having a form of thick bed. Since salt is a diamagnetic material with very low negative magnetization (= –10 mA/m) usually occurring in a host media with low magnetization (here a magnetization of 30 mA/m was selected), the amplitude of the modeled

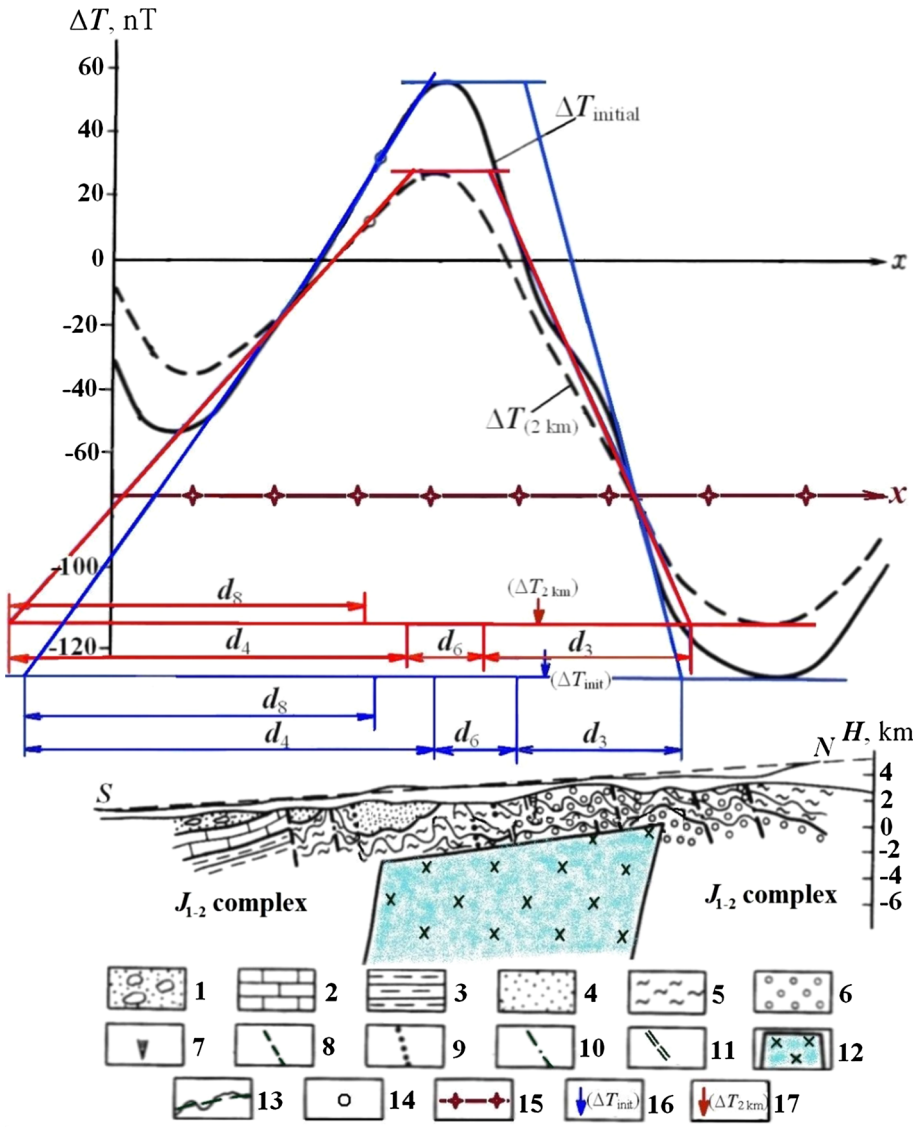

Fig. 10 Interpretation of ΔT graphs on two levels along profile through the Guton anomaly (Azerbaijan, southern slope of the Greater Caucasus). *1* recent alluvial deposits; *2* limestone, tuff sandstone, clay shale (*K*); *3* mudstone, tuff sandstone (J_3); *4* clay shale and coarse-grained tuff sandstone (J_2); *5* sandy-clay shale, a sand flysch, metamorphosed clay shale and sandstone (J_2); *6* phyllitizated clay shale, sandstone, and spilite (J_1); *7* dikes and sheet bodies of the gabbro–diabasic association (J_2); *8* regional upthrust–overthrusts; *9* upthrust–overthrusts separating the longitudinal tectonic steps of the second order; *10* upthrust–overthrusts complicating the longitudinal tectonic steps; *11* transverse fractures; *12* magmatic intrusion of intermediate-acid composition according to the performed analysis and other geological–geophysical data (non-segmented J_{1-2} complex); *13* the line of airborne magnetic survey and averaging inclined straight line; *14* inflection point of the plot ΔT closest to the maximum on the *left*; *15* corrected zero line of the plots ΔT; determined position of the center of *upper edge* of thick bed by the analysis of: *16* ΔT_{init} (airborne observations); *17* ΔT upward analytically continued to 2 km. *Blue* and *red* tangents and intervals relate to ΔT_{init} and $\Delta T_{(2\text{ km})}$, respectively

anomaly is only about 3 nT. The characteristic peculiarity of this model is the presence of a rugged terrain relief disturbing the magnetic anomaly. The results of quantitative interpretation do not ideally coincide with the PGM, but demonstrate sufficient accuracy (Fig. 8); the calculated J_e value was about -7 mA/m.

Finally, let us consider the magnetic effect from the "classic" thin horizontal plate characterized by large horizontal thickness $2b$, small vertical thickness ($2b \gg h_1$ and h_2), and near-surface occurrence. Of course, this model cannot be interpreted as a "quasi-thick" model. If the parameter $2b$ is sufficiently large, we observe two independent anomalies that we can interpret using methodologies developed for complex physical–geological conditions for the model of thin bed (Eppelbaum et al. 2001). In this case, we assume that the magnetization of the left-hand bed is positive, and the right-hand bed is a negative one (in this case, determining the magnetization is not possible). As

shown in Fig. 9, the results of the interpretation indicate the position of the center of the upper edges of two "fictitious" thin beds in the left (positive anomaly) and right (negative anomaly) of the considered thin horizontal plate model.

Field examples

The aforementioned methodology of magnetic anomaly examination was successfully applied to many field examples. Let us consider one case of regional magnetic data analysis (the southern slope of the Greater Caucasus) and one very detailed case from archeological geophysics.

Guton magnetic anomaly of the Greater Caucasus

We will consider here an example of the Guton magnetic anomaly situated in NW Azerbaijan (the southern slope of the Greater Caucasus), near the border with Russia. A detailed quantitative interpretation of this anomaly was carried out along 15 profiles crossing it. The results along one of the profiles (the anomalous body was approximated by a thick inclined bed) are presented in Fig. 10 (here, improved tangent, characteristic point, and areal methods were applied). The data indicate that the anomalous body is characterized by comparatively low magnetization ($J = 250$ mA/m), considerable vertical thickness (about 30 km) and a steep dip of the lateral contacts; analytical continuation and singular point methods applied on the same profiles gave similar results. The characteristics of this anomalous body prove the intermediate-acid composition of this target (intrusion). The interpretation of the significant vertical thickness of this body agrees with the geothermic data on the depth of the Curie discontinuity in this area (about 30 km) (Eppelbaum et al. 2014). The outcroppings at the Earth's surface formed sub-volcanic and sub-intrusive bodies of various consistencies that are apparently fragments of this large magmatic massif penetrating the upper part of the section along the extended faults of the common Caucasian direction. The magmatic focus shown is associated with the rich pyrite–polymetallic deposits of the Zagatala-Belokan ore field and possibly other areas in the Greater Caucasus (Eppelbaum and Khesin 2012). Thus, the data presented in Fig. 10 give a good example of an integrated PGM.

Banias site of the Roman period (northern Israel)

The remains of the city of Banias (Roman period) are located in northern Israel, at the foot of Mt. Hermon. In the vicinity nearest the area of the geophysical investigations described here, the remains of a Roman cemetery and aqueduct (Hartal 1997) have been discovered. Petrological

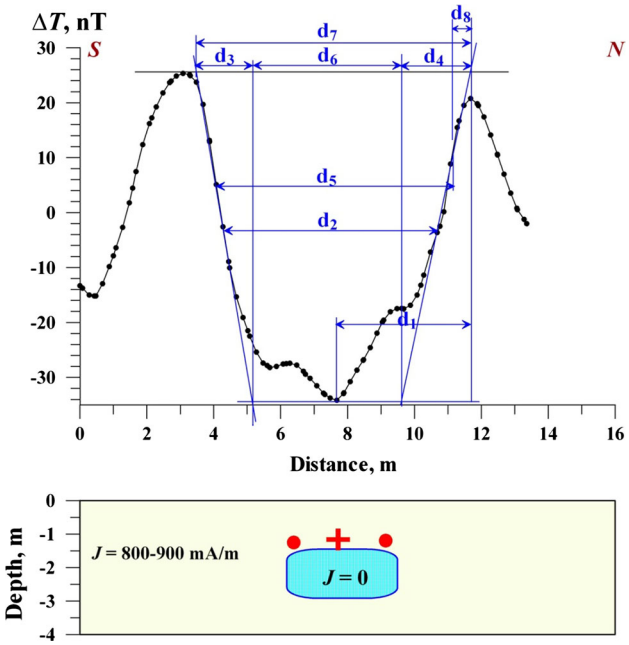

Fig. 11 Interpretation of magnetic anomaly from buried Roman chamber, northern continuation of the Banias site (foot of Mt. Hermon, northern Israel) (initial data according to Eppelbaum et al. 2003)

and petrophysical analyses of the excavated chambers indicated that these objects were built from a special type of limestone ($J = 0$–2 mA/m) that is found in the host media of basaltic pebbles and magnetic soil ($J = 800$–900 mA/m). Quantitative interpretation of the observed negative anomaly using the above-mentioned methodology has shown that obtained position of the thick bed is at a lowered depth compared with the results of archeological excavations (Fig. 11); apparently it is caused by the essential inhomogeneity of the host media.

Conclusions

An interpretation methodology (improved characteristic point and tangent methods) for analyzing magnetic anomalies produced by the thick bed model in complex physical–geological conditions (oblique magnetization, rugged terrain relief and absence of knowledge of normal magnetic field level) is presented in detail. The application of this methodology allows for precisely determining the position of the upper edge (surface) of the target under study, as well as some other parameters. An important conclusion about the applicability of this methodology for quantitative interpretation of magnetic anomalies from bodies occupying intermediate geometric forms between the thick bed and thin horizontal plate was done. It allows to significantly increase an interpretation potential of this

methodology. In the case of a thin plate model with a large horizontal distance $2b$ between the left and right edges, these two anomalies may be independently interpreted as typical anomalies from vertical thin beds. Several models (PGM of intrusive bodies and salt layer were used) and field examples (regional magnetic data examination from granitic intrusive in the southern slope of the Greater Caucasus and interpretation of magnetic anomaly from a Roman archeological site in Northern Israel) demonstrate the effectiveness of applying this methodology; its integration with known rapid interpretation methods (Euler deconvolution, analytic signal, wavelet transform, etc.) in complex geological situations may greatly increase the accuracy of the magnetic data quantitative analysis. Further elaboration of the presented methodology will include the development of a software package for formalization of the interpreting process.

Acknowledgments The author would like to thank two anonymous reviewers and the editor-in-chief, who thoroughly reviewed the manuscript, and whose critical comments and valuable suggestions were very helpful in preparing this paper.

References

Am K (1972) The arbitrarily magnetized dyke: interpretation by characteristics. Geophys Explor 10:63–90

Beiki M (2013) TSVD analysis of Euler deconvolution to improve estimating magnetic source parameters: an example from the Åsele area, Sweden. J Appl Geophys 90:82–91

Blakely RJ (1995) Potential theory in gravity and magnetic applications. Cambridge University Press, Cambridge

Bulina LV (1970) Peculiarities of space distribution of the magnetized formations lower edges for consolidated Earth crust. Izvestiya Acad Sci USSR, Ser Geol 5:70–75 **(in Russian)**

Chianese D, Lapenna V (2007) Magnetic probability tomography for environmental purposes: test measurements and field applications. J Geophys Eng 4:63–74

Davis K, Li Y, Nabighian M (2010) Automatic detection of UXO magnetic anomalies using extended Euler deconvolution. Geophysics 75(3):G13–G20

Dukhovsky AA, Ilayev MG, Kronidov II (1970) Geophysical investigations. Methodological instructions for geological survey on a 1:50,000 scale. Nedra, Leningrad **(in Russian)**

Eppelbaum LV (2006) Methodology of 3-D combined modeling of magnetic and gravity fields in the Eastern Mediterranean. In: Proceedings of the 3rd EUG meeting, Vienna, Vol. 8, 02057, pp 1–4

Eppelbaum LV (2011) Study of magnetic anomalies over archaeological targets in urban conditions. Phys Chem Earth 36(16):1318–1330

Eppelbaum LV, Katz YuI (2015) Newly developed Paleomagnetic Map of the Easternmost Mediterranean Unmasks geodynamic history of this region. Open Geosci 7(1):95–117 **(Springer)**

Eppelbaum LV, Khesin BE (2001) Disturbing factors in geophysical investigations at archaeological sites and ways of their elimination. In: Proceedings of the IV conference on archaeological prospection, Vienna, pp 99–101

Eppelbaum LV, Khesin BE (2012) Geophysical studies in the Caucasus. Springer, Berlin

Eppelbaum LV, Mishne AR (2011) Unmanned airborne magnetic and VLF investigations: effective geophysical methodology of the near future. Positioning 2(3):112–133

Eppelbaum LV, Khesin BE, Itkis SE (2001) Prompt magnetic investigations of archaeological remains in areas of infrastructure development: Israeli experience. Archaeol Prospect 8(3):163–185

Eppelbaum L, Ben-Avraham Z, Itkis S (2003) Ancient Roman Remains in Israel provide a challenge for physical-archaeological modeling techniques. First Break 21(2):51–61

Eppelbaum LV, Khesin BE, Itkis SE (2010) Archaeological geophysics in arid environments: examples from Israel. J Arid Environ 74(7):849–860

Eppelbaum LV, Kutasov IM, Pilchin AN (2014) Applied geothermics. Springer, Berlin

Flanagan G, Bain JE (2013) Improvements in magnetic depth estimation: application of depth and width extent nomographs to standard depth estimation techniques. First Break 31(12):41–51

Florio G, Fedi M (2014) Multiridge Euler deconvolution. Geophys Prospect 62(2):333–351

Fregoso E, Gallardo LA, García-Abdeslem J (2015) Structural joint inversion coupled with Euler deconvolution of isolated gravity and magnetic anomalies. Geophysics 80(2):G67–G79

Hartal M (1997) Banias, the Aqueduct. Excav surv Israel 16:5–8

Ialongo S, Fedi M, Florio G (2014) Invariant models in the inversion of gravity and magnetic fields and their derivatives. Appl Geophys 110:51–62

Khesin BE, Alexeyev VV, Eppelbaum LV (1996) Interpretation of geophysical fields in complicated environments. Kluwer Academic Publ. (Springer), Ser.: Modern approaches in geophysics

Logachev AA, Zakharov VP (1973) Magnetic prospecting. Nedra, Sankt-Petersburg **(in Russian)**

Moreau F, Gibert D, Saracco G, Holschneider M (1999) Identification of sources of potential fields with the continuous wavelet transform—basic theory. J Geophys Res 104(B3):5003–5013

Nabighian MN (1972) The analytic signal of two-dimensional magnetic bodies with polygonal cross-section: its properties and use for automated anomaly interpretation. Geophysics 37:507–517

Nikitsky VE, Glebovsky YuS (eds) (1990) Magnetic prospecting. Nedra, Moscow **(in Russian)**

Parasnis DS (1997) Principles of applied geophysics. Chapman & Hall, London

Peters LJ (1949) The direct approach to magnetic interpretation and its practical applications. Geophysics 14:290–320

Phillips JD, Hansen RO, Blakely RJ (2007) The use of curvature in potential-field interpretation. Explor Geophys 38(2):111–119

Pilchin AN, Eppelbaum LV (1997) Determination of magnetized bodies lower edges by using geothermal data. Geophys J Inter 128(1):167–174

Pyatnitsky VK (1961) On the maximum slope method. In: Proceedings of the Institute of geology and geophysics, USSR Academy of Science, Siberian Branch, 11, pp 109–120 **(in Russian)**

Rao DA, Babu HV (1984) On the half-slope and straight-slope methods of basement depth determination. Geophysics 49(8):1365–1368

Ravat D, Taylor PT (1998) Determination of depths to centroids of three-dimensional sources of potential-field anomalies with examples from environmental and geologic applications. J Appl Geophys 39:191–208

Reford MS, Sumner JS (1964) Aeromagnetics. Geophysics 29:482–516

Reid AB, Allsop JM, Granser H, Millet AJ, Somerton IW (1990) Interpretation in three dimensions using Euler deconvolution. Geophysics 55(1):80–91

Roest WR, Verhoef J, Pilkington M (1992) Magnetic interpretation using the 3-D analytic signal. Geophysics 57(1):116–125

Salem A, Ravat D, Smith R, Ushijima K (2005) Interpretation of magnetic data using an enhanced local wavenumber (ELW) method. Geophysics 70(2):L7–L12

Stampolidis A, Tsokas GN (2012) Use of edge delineating methods in interpreting magnetic archaeological data. Archaeol Prospect 19:123–140

Stroud KA (2001) Engineering mathematics, 5th edn. PALGRAVE, Basingstoke

Tafeyev YuP, Sokolov KP (1981) Geological interpretation of magnetic anomalies. Nedra, Leningrad **(in Russian)**

Telford WM, Geldart LR, Sheriff RE (1990) Applied geophysics. Cambridge University Press, Cambridge

Troshkov GA, Groznova AA (1985) Mathematical methods of magnetic anomaly interpretation. Nedra, Moscow **(in Russian)**

Vallée MA, Keating P, Smith RS, St-Hilaire C (2004) Estimating depth and model type using the continuous wavelet transform of magnetic data. Geophysics 69:191–199